SiO_2 stishovite under high pressure: Dielectric and dynamical properties and the ferroelastic phase transition

Changyol Lee
Department of Physics, Ewha Womans University, Seoul 120-750, South Korea

Xavier Gonze
Unité de Physico-Chimie et de Physique des Matériaux, Université Catholique de Louvain, B-1348 Louvain-la-Neuve, Belgium
(Received 11 November 1996; revised manuscript received 5 June 1997)

The pressure dependence of the dielectric and dynamical properties of SiO_2 stishovite and its pressure-induced ferroelastic phase transition to the $CaCl_2$ structure are investigated using density-functional theory. The pressure dependence of the dielectric permittivity tensors and the Born effective charges shows that the local atomic environments in stishovite, more compressible along the *a* axis than along the *c* axis, become less anisotropic as pressure increases. The phonon frequencies at the Γ point increase with increasing pressure, except the B_{1g} mode. The phonon band structure at 73 GPa, the study of elastic constants as a function of pressure, and the structural relaxation at various pressure provide evidence for spontaneous elastic deformation, i.e., a ferroelastic phase transition at 64 GPa of stishovite in the tetragonal rutile structure to the orthorhombic $CaCl_2$ structure. The on-site and interatomic force constants are found to be consistent with the predicted structural phase transition. The dielectric properties and the phonon frequencies at the Γ point are also computed in the $CaCl_2$ structure. [S0163-1829(97)03636-9]

I. INTRODUCTION

Many crystalline polymorphs of silicon dioxide (SiO_2) have been found in nature, or synthesized in laboratory. At ambient pressure, SiO_2 polymorphs α and β quartz, tridymite S, and β cristobalite are known to be stable in different ranges of temperature.[1] α quartz transforms to coesite for pressures between 1.5 and 4 GPa.[1,2] Tridymite S and β cristobalite also transform to coesite under pressure. Coesite undergoes a phase transition to stishovite at about 8 GPa.[3,4] The coesite-to-stishovite transition is accompanied by a rather large volume decrease, because the coordination number of Si changes from 4 in coesite to 6 in stishovite. At the depth of 1200 km, the pressure in the Earth's mantle, where Si, O, and Mg are the most abundant elements, is about 50 GPa. Therefore, knowledge of the high-pressure behavior of SiO_2, therefore, is essential to understand the internal constitution of the Earth. It can also shed light on the physical and chemical properties and the interactions among the major components of the Earth.

The structural and dielectric properties and the lattice dynamics of SiO_2 polymorphs have been the subject of many experimental and theoretical research. The thermodynamic properties and the equilibrium phase relations have also been studied (see, for example, Refs. 5–8). Compared to the other low-pressure SiO_2 polymorphs, the experimental characterization of the dielectric and lattice-dynamical properties of stishovite have been relatively limited, as the available monocrystals of stishovite, metastable at ambient pressure, are very small. We studied the dielectric and lattice-dynamical properties of stishovite at ambient pressure with theoretical methods based on the density-functional perturbation theory (DFPT). A detailed account of DFPT is presented in Refs. 9 and 10, while the ambient-pressure results are presented in Ref. 11.

The pressure dependence of the dielectric and dynamical properties of stishovite were even less investigated experimentally. High-pressure x-ray diffraction data[12] and the pressure dependence of infrared[7] and Raman[13,14] spectra of stishovite have been reported. However, except a brief account of the present theoretical work,[15] the dielectric permittivity tensors and the phonon frequencies at arbitrary wave vectors have not been reported as a function of pressure.

The dielectric properties of solids are strongly related to the atomistic interaction and their knowledge is valuable to the study of the structural properties. The *ab initio* theoretical methods, which assume no experimental inputs, can provide information on the pressure dependence of the dielectric properties of stishovite, where the experimental data are lacking. These methods can also facilitate the understanding of the interaction between atoms, and the nature of still another pressure-induced phase transition.

Indeed, stishovite undergoes another pressure-induced phase transition, which has intrigued geophysicists and geochemists. Theoretical and experimental work suggested transitions to the fluorite (CaF_2) structure,[16] the pyritelike ($Pa\bar{3}$) structure,[17] the α-PbO_2 structure,[18,19] the hexagonal Fe_2N structure[20,21] or the orthorhombic $CaCl_2$ structure[12,14,22–28] with a wide range of transition pressure.

In this work, we calculate the equation of state, the structural parameters of stishovite for a range of pressures (0, 18, 42, 73, and 114 GPa), as well as the corresponding high-frequency and low-frequency dielectric permittivity tensors, the Born effective charges, the phonon frequencies at the Γ point of stishovite in the rutile structure. The phonon band structure and the real-space interatomic force constants (IFC's) at 0 and 73 GPa are also calculated and compared. The phonon frequencies and the elastic properties are closely investigated to study the possible instability-driven phase

TABLE I. Violation of the charge-neutrality sum rule of the Born effective charge tensors with respect to the **k** point sampling. The components not shown satisfy the neutrality sum rule.

Monkhorst-Pack grid	$\sum_\kappa Z^*_{\kappa,xx}$, $\sum_\kappa Z^*_{\kappa,yy}$	$\sum_\kappa Z^*_{\kappa,zz}$
$(2\times2\times2)$	−0.168	3.435
$(2\times2\times4)$	−0.071	0.249
$(2\times2\times6)$	−0.077	0.037
$(4\times4\times4)$	−0.024	0.276

transition: we observe a second-order transition to the $CaCl_2$ structure at about 64 GPa, driven by mechanical instability. The relaxation of the structural degrees of freedom is performed at various values of pressure and the dielectric properties of the relaxed structure are calculated.

The remaining part of this paper is organized as follows. In Sec. II, we describe the technical details of our calculation including an analysis of the numerical convergence. Results are presented in Sec. III. From Secs. III A to III E, we present the equation of state, the pressure dependence of the dielectric permittivity tensors, the Born effective charge tensors, the phonon frequencies at the Γ point of stishovite under the assumption that the tetragonal rutile structure is stable at the pressure of investigation. From Secs. III F to III H, we study the structural phase transition of stishovite and the dielectric properties of the relaxed structure. We summarize and conclude in Sec. IV.

II. CALCULATIONAL METHODS

A. Density-functional perturbation theory

The DFT, in the local density approximation[29] (LDA) accurately describes the properties of condensed matter systems in their electronic ground state.[30] Their responses to external perturbations, like homogeneous electric fields or atomic displacements, have been calculated within the LDA using various methods.[9,10,31] In the variational approach to the DFPT that we have elaborated in Refs. 9 and 10, an efficient minimization technique facilitates the self-consistent evaluation of the derivatives of the wave functions and energy. The DFPT makes it easy to handle perturbations incommensurate with the periodic lattice, or homogeneous electric fields whose potential is linear in space and breaks the translational symmetry of the problem. The DFPT has been used in prior studies on SiO_2,[32–34] TiO_2,[35,36] Si,[37] and $BaTiO_3$.[38]

B. Implementation of DFT and input parameters

DFT calculations are performed using a plane-wave basis set and accurate *ab initio* pseudopotentials. A rational polynomial parametrization of the Ceperley-Alder exchange-correlation energy[39] ensures the continuity of the exchange-correlation potential and its derivatives over all the electron density. Conjugate-gradient algorithms (Ref. 40 for the ground state, Ref. 9 for the response functions) are used to solve the minimization problems.

Chemical hardness-conserving, extended norm-conserving, pseudopotentials[41] describe the Si and O atom interaction with valence electrons. The cutoff radii for Si and O pseudopotentials are 2.0 and 1.5 a.u., respectively.

The maximum kinetic energy of the plane waves included in the basis set is 30 Hartree. With this cutoff, structural data of α quartz were converged well within 1%.[32]

The convergences of the calculated physical properties with respect to the **k**-point sampling of the electronic wavefunctions in the BZ were studied with Monkhorst-Pack[42] grids of $(2\times2\times2)$, $(2\times2\times4)$, $(2\times2\times6)$, and $(4\times4\times4)$ special **k** points, respectively, reducing to 1 special **k** point $[(\frac{1}{4},\frac{1}{4},\frac{1}{4})]$, 2 special **k** points $[(\frac{1}{4},\frac{1}{4},\frac{1}{8})$ and $(\frac{1}{4},\frac{1}{4},\frac{3}{8})]$, 3 special **k** points $[(\frac{1}{4},\frac{1}{4},\frac{1}{12})$, $(\frac{1}{4},\frac{1}{4},\frac{1}{4})$, and $(\frac{1}{4},\frac{1}{4},\frac{5}{12})]$, 6 special **k** points $[(\frac{1}{8},\frac{1}{8},\frac{1}{8})$, $(\frac{1}{8},\frac{3}{8},\frac{1}{8})$, $(\frac{3}{8},\frac{3}{8},\frac{1}{8})$, $(\frac{1}{8},\frac{1}{8},\frac{3}{8})$, $(\frac{1}{8},\frac{3}{8},\frac{3}{8})$, and $(\frac{3}{8},\frac{3}{8},\frac{3}{8})]$ in the irreducible BZ, when the full symmetry of the space group can be used, as in the ground-state calculations. For the structural parameters, agreement within 0.3% was obtained between the sets of 3 and 6 special **k** points.

Of course, one cannot sample only the irreducible part of the BZ with symmetry-breaking perturbations, for which the

TABLE II. The structural parameters of stishovite at zero pressure. a and c are the lattice constants and u is the internal coordinates of the O atoms. V_0 is the volume of the unit cell, B_0 is the bulk modulus, B_0' is the pressure derivative of the bulk modulus at zero pressure.

	a (Å)	c (Å)	u (in a)	V_0 (Å^3)	B_0 (GPa)	B_0'
			Theory			
This work	4.14	2.66	0.305	45.54	319.6	3.87
Ref. 28	4.157	2.658	0.3058	45.92	313	4.24
Ref. 55	4.20	2.65	0.306	46.75	286	4.6
Ref. 56	4.195	2.677	0.3061	47.50	286	3.72
Ref. 25	4.15	2.69	0.306	46.2	328	4.00
Ref. 45	4.14	2.67	0.305	45.64	292.0	5.86
Ref. 62	4.255	2.604	0.3082	47.145		
			Experiment			
Ref. 57	4.1801	2.6678	0.3067	46.615	313.0	1.7
Ref. 58	4.1773	2.6655	0.30608	46.51		
Ref. 59	4.1772	2.6651	0.3062	46.503		
Ref. 60	4.1812	2.6660		46.61	288	
Ref. 61	4.180	2.666		46.58	344	5.7

full Monkhorst-Pack grid must be used. See Refs. 9 and 10 for the analysis of the effect of symmetry on the implementation and computational load of the algorithms. We have monitored the convergence of the charge neutrality sum rule (see Table I) then checked the convergence of some phonon frequencies with the charge neutrality sum rule enforced as in Eq. (48) of Ref. 10. The phonon frequencies agree within 0.5% between the calculations with sets of 3 and 6 special **k** points. Therefore, we use the set of 3 special **k** points for further calculations.

C. The parameters for dynamical properties

Dynamical matrices are computed *ab initio* for **q** wave vectors belonging to the $(1\times1\times1)$, $(2\times2\times2)$, $(2\times2\times4)$ Monkhorst-Pack grids, respectively. Then, their short-range parts are Fourier transformed, in order to generate the real-space IFC's.[34,10] These grids correspond to real-space boxes containing 6, 48, and 96 atoms, respectively. The long-range dipole-dipole interaction is described by an analytical expression (see Ref. 34). The symmetries of the full space group, as well as the time-reversal symmetry can be used to decrease the number of **q** wave vectors, in the same way as, in unperturbed systems, the electronic wave functions can be generated only for the **k** wave vectors contained in the irreducible BZ. The above three Monkhorst-Pack grids reduce to 1 special **q** point $[(0,0,0)]$, 1 special **q** point $[(\frac{1}{4},\frac{1}{4},\frac{1}{4})]$, and 2 special **q** points $[(\frac{1}{4},\frac{1}{4},\frac{1}{8})$ and $(\frac{1}{4},\frac{1}{4},\frac{3}{8})]$. The phonon frequencies generated from the $(2\times2\times4)$ IFC's show agreement within 2% error to those calculated directly at high-symmetry **q** points in the BZ including Z, X, M, R, and A.[43] Sparser grids $(1\times1\times1)$ and $(2\times2\times2)$ lead to 17 and 3% errors, respectively.

III. RESULTS

A. The equation of state

Stishovite has a tetragonal unit cell with Si atoms at $(0,0,0)$ and $(\frac{1}{2},\frac{1}{2},\frac{1}{2})$ and O atoms at $(u,u,0)$, $(1-u,1-u,0)$, $(\frac{1}{2}-u,\frac{1}{2}+u,\frac{1}{2})$, and $(\frac{1}{2}+u,\frac{1}{2}-u,\frac{1}{2})$, in the unit of lattice constants. This is known as the rutile structure; its space group is D_{4h}^{14} $(P4_2/mnm)$. The structure is completely determined by the lattice constants a and c and an internal parameter u. We calculate the minimum-energy configuration of the unit cell with respect to a, c, and u for a given volume, assuming the rutile structure is the lowest-energy configuration in the range of pressure studied. The total energies of the optimized geometries with various volumes are fitted into Murnaghan equation of state[44] of the following form:

$$E=\frac{V_0B_0}{B_0'}\left[\frac{1}{B_0'-1}\left(\frac{V_0}{V}\right)^{B_0'-1}+\frac{V}{V_0}\right]+\text{const}, \qquad (1)$$

where E is the total energy per unit cell and V is the volume of the unit cell. We obtain from the fitted equation of state the equilibrium volume V_0, the bulk modulus B_0, and the pressure derivative of bulk modulus B_0' at zero pressure, as shown in Table II. The agreement between our calculated and the experimental values is good, with slight underestimation of the relative volume at high pressure as shown in Fig. 1. The calculated structural parameters and equation of state will be used for further investigation. It should be noted that experimental values of B_0' have a wide range.[45] In Table III, we show the unit-cell volume and other structural parameters as a function of pressure. It can be seen that stishovite is more compressible along the a axis than along the c axis, like other rutile-structured compounds.[46] The internal parameter u decreases with increasing pressure, indicating the contraction of Si-O bond lengths from 1.26 Å at 0 GPa to 1.14 Å at 114 GPa.

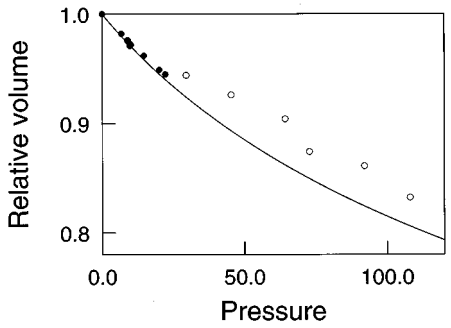

FIG. 1. The calculated equation of state (solid line) of stishovite. Filled and open circles are experimental data from Refs. 61 and 12, respectively. The pressure is in GPa.

The assumption that the rutile structure is energetically favored in stishovite up to 114 GPa will be maintained in Sec. III B through Sec. III E, although a structural phase transition to the $CaCl_2$ structure will be found to occur well below 114 GPa. The structural phase transition will be a major point of study and the dielectric properties of stishovite in the relaxed $CaCl_2$ structure will be discussed in later sections.

B. The pressure dependence of the dielectric permittivity tensors and Born effective charges

Next, we calculate the pressure dependence of the high-frequency (electronic) dielectric permittivity tensor (ϵ_{ij}^{∞}), the low-frequency (static) dielectric permittivity tensor (ϵ_{ij}^{0}), and the Born effective charge tensors ($Z_{\tau,ij}^{*}$) where i and j are the x, y, or z axis and τ is the Si or O atom. Stishovite is assumed to have the rutile structure and the dielectric properties are calculated up to 114 GPa. ϵ_{ij}^{0} at 114 GPa is not defined because it includes the contributions from ionic displacement and one of the ionic displacement modes has an

TABLE III. The calculated equation of state of stishovite and the pressure dependence of the structural parameters of stishovite. The rutile structure is assumed.

Pressure (GPa)	Volume (Å^3)	a (Å)	c (Å)	u (in a)	c/a
0	45.5	4.14	2.66	0.3052	0.6421
18	43.3	4.06	2.63	0.3036	0.6471
42	41.0	3.98	2.59	0.3024	0.6503
73	38.7	3.90	2.54	0.3014	0.6524
114	36.4	3.82	2.50	0.3005	0.6537

TABLE IV. The high-frequency and low-frequency dielectric permittivity tensors (ϵ^{∞}_{ii} and ϵ^{0}_{ii}, respectively), the Born effective charge tensors (Z^{*}_{ij} and their principal values ζ^{*}_{i}) as a function of pressure. The indices in ϵ^{∞}_{ii}, ϵ^{0}_{i}, and Z^{*}_{ij} are x, y, or z and the index in ζ^{*}_{i} runs over the principal axes 1, 2, and 3. The rutile structure is assumed unless otherwise stated. The components not shown are zero.

Pressure (GPa)	0	18	42	73	114	73[a]
			Dielectric permittivity tensors			
ϵ^{∞}_{xx}, ϵ^{∞}_{y}	3.306	3.249	3.200	3.159	3.126	3.169, 3.174
ϵ^{∞}_{zz}	3.502	3.449	3.397	3.349	3.305	3.370
ϵ^{0}_{xx}, ϵ^{0}_{yy}	11.014	9.697	8.854	8.273	Not defined	8.179, 8.406
ϵ^{0}_{zz}	9.144	8.630	8.074	7.535	Not defined	7.752
			Born effective charge			
$Z^{*}_{\mathrm{Si},xx}$, $Z^{*}_{\mathrm{Si},yy}$	3.803	3.776	3.748	3.719	3.689	3.662, 3.785
$Z^{*}_{\mathrm{Si},xy}$, $Z^{*}_{\mathrm{Si},yx}$	0.343	0.303	0.269	0.238	0.211	0.312, 0.158
$Z^{*}_{\mathrm{Si},zz}$	4.055	4.025	3.993	3.958	3.922	3.954
$\zeta^{*}_{\mathrm{Si},1}$	4.143	4.079	4.017	3.957	3.900	3.954
$\zeta^{*}_{\mathrm{Si},2}$	3.460	3.473	3.479	3.481	3.478	3.493
$\zeta^{*}_{\mathrm{Si},3}$	4.055	4.025	3.993	3.958	3.923	3.954
$Z^{*}_{\mathrm{O},xx}$, $Z^{*}_{\mathrm{O},yy}$	−1.902	−1.888	−1.874	−1.859	−1.845	−1.831, −1.893
$Z^{*}_{\mathrm{O},xy}$, $Z^{*}_{\mathrm{O},yx}$	−0.557	−0.534	−0.511	−0.488	−0.466	−0.488, −0.487
$Z^{*}_{\mathrm{O},zz}$	−2.119	−2.013	−1.996	−1.979	−1.961	−1.977
$\zeta^{*}_{\mathrm{O},1}$	−2.459	−2.422	−2.395	−2.347	−2.311	−2.350
$\zeta^{*}_{\mathrm{O},2}$	−1.345	−1.354	−1.363	−1.371	−1.379	−1.374
$\zeta^{*}_{\mathrm{O},3}$	−2.119	−2.013	−1.996	−1.979	−1.961	−1.977

[a]In $CaCl_2$ structure.

imaginary frequency (see Sec. III C). Because of the tetragonal symmetry of the structure, only two components of the dielectric permittivity tensor are independent, ϵ_{xx} and ϵ_{zz}: the off-diagonal components vanish, while $\epsilon_{xx}=\epsilon_{yy}$.

The summarized results are shown in Table IV. As pressure increases, both ϵ^{∞}_{ii} and ϵ^{0}_{ii} decrease. From 0 GPa to 73 GPa, the lattice constants a decrease by 5.8% and c by 4.5%, while ϵ^{∞}_{xx} and ϵ^{∞}_{zz} decrease by 4.4% and ϵ^{0}_{xx} decrease by 24.9% and ϵ^{0}_{zz} decrease by 17.6%. $\epsilon^{\infty}_{xx}/\epsilon^{\infty}_{zz}$ is 1.06 from 0 to 73 GPa, whereas $\epsilon^{0}_{xx}/\epsilon^{0}_{zz}$ decreases from 1.20 at 0 GPa to 1.10 at 73 GPa.

Each $Z^{*}_{\tau,ij}$ decreases as pressure increases. $Z^{*}_{\mathrm{Si},xx}$, $Z^{*}_{\mathrm{Si},xy}$, and $Z^{*}_{\mathrm{Si},zz}$ decrease by 2.2, 31.6, and 2.4%, respectively, and $Z^{*}_{\mathrm{O},xx}$, $Z^{*}_{\mathrm{O},xy}$, and $Z^{*}_{\mathrm{O},zz}$ decrease by 2.3, 12.4, and 6.6%, respectively, as the pressure increases from 0 to 73 GPa. When the axes are chosen along and perpendicular to the bond direction in the x-y plane, $Z^{*}_{\tau,ij}$ can be diagonalized, with the principal values ζ^{*}_{i} as the diagonal elements. $(\zeta^{*}_{1}-\zeta^{*}_{2})/\zeta^{*}_{3}$, the difference between the largest and the smallest ζ^{*}_{i} over ζ^{*}_{3} change from 16.5 to 12.1% for Si atoms and from 45.3 to 41.6% for O atoms, i.e., $Z^{*}_{\tau,ij}$ becomes less anisotropic at higher pressures. The decrease in anisotropy can be understood by the fact that the unit cell becomes more compressed along the a axis and closer to the cubic structure.

C. The pressure dependence of the phonon frequencies at the Γ point

We also investigate the phonon frequencies of stishovite at the Γ point. Stishovite is assumed to have the rutile structure and the phonon frequencies are calculated at 0, 18, 42, 73, and 114 GPa. The frequency of the Raman-active B_{1g} mode decreases with increasing pressure, whereas the frequencies of all the other phonon modes increase, as shown in Figs. 2 and 3. The order of some phonon frequencies changes as pressure increases. The experimental values of the pressure shifts of the phonon frequencies also agree well with our calculated pressure shifts which appear in Table 2 of Ref. 47.

Interpolation leads to vanishing phonon frequency of the B_{1g} mode at 86 GPa, as shown in Fig. 1 of Ref. 47. Therefore, stishovite is unstable above 86 GPa with respect to the

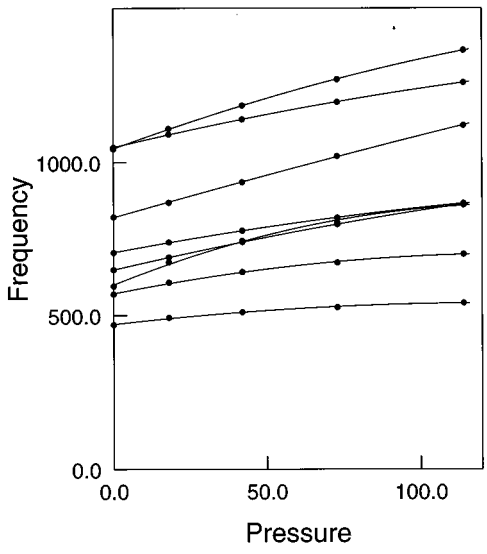

FIG. 2. The phonon frequencies of the infrared-active modes as a function of pressure. The frequencies are in cm^{-1} and the pressure is in GPa.

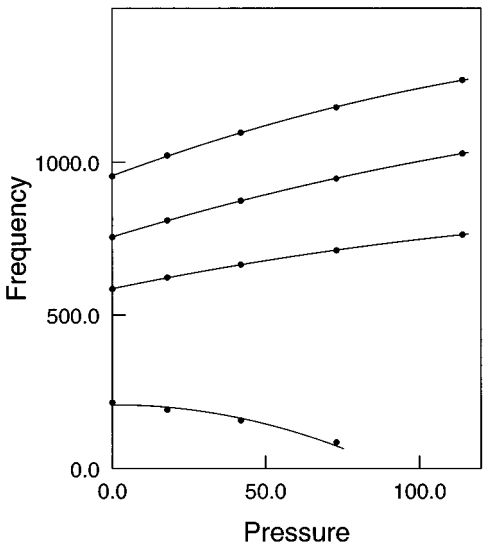

FIG. 3. The phonon frequencies of the Raman-active modes as a function of pressure. The frequencies are in cm^{-1} and pressure is in GPa.

atomic displacements characteristics of the B_{1g} mode. (The B_{1g} displacements are the rigid rotation of the O octahedra around Si atoms within a-b plane.) However, it is not guaranteed that stishovite is stable below 86 GPa with respect to other instabilities. The relation of the instability due to the softening of the B_{1g} mode to the phase transition at high pressure will be elaborated in Sec. III F.

D. The phonon band structure at 0 and 73 GPa

We computed the phonon spectra over the entire Brillouin zone of stishovite in the rutile structure at 0 and 73 GPa. The technique that we followed is explained carefully in Ref. 10, and summarized hereafter. We computed first the dynamical matrices on a (2,2,4) Monkhorst-Pack grid in the reciprocal space. Then, we separated the dynamical matrices into two terms, one from the long-range dipole-dipole interaction and the other from the remaining short-ranged interaction. The short-ranged interaction part is interpolated thanks to a Fourier transform to real-space IFC's, followed by inverse Fourier transform to any wavevector dynamical matrix. The long-range dipole-dipole interactions are taken into account using an analytical expression based on the calculated anisotropic Born effective charge tensors and the dielectric permittivity tensors. The combined dynamical matrices can be interpolated at arbitrary wavevectors and generate the full phonon spectra.

The phonon band structures at 0 and 73 GPa are shown in Fig. 2 of Ref. 47. The phonon frequencies at 73 GPa have a wider range than those at 0 GPa and the frequency of the B_{1g} mode at and near the Γ point significantly approaches to zero. All the modes (except the three acoustic modes at the Γ point) have positive frequencies at any point in the BZ at 0 GPa. At 73 GPa, the same holds with the important exception of an acoustic mode along the Γ-M line around the long-wavelength limit. The imaginary frequency of this acoustic mode implies that the rutile structure at 73 GPa is unstable with respect to some long-wavelength mechanical perturbation. So, the pressure region in which stishovite is unstable is brought down from 86 GPa and over to 73 GPa and over. The acoustic modes along the Γ-M line are the ones with wave vectors $\mathbf{q}$ such that $q_x = q_y$ and $q_z = 0$. In the long-wavelength limit, these acoustic modes corresponds to a uniform compression in the a-b plane if the atomic motions in the x and y direction are in phase or to a shear distortion in the a-b plane if out of phase.[48] Our calculated bulk modulus at 73 GPa is 598.0 GPa and positive, therefore stishovite is stable under the uniform compression. We describe in Sec. III F the instability of stishovite under the shear distortion.

E. The IFC's at 0 and 73 GPa

Let us now compare the *ab initio* IFC tensors of stishovite in the rutile structure at 0 and 73 GPa, shown in Table V and Table VI, respectively.

The real-space IFC $\Phi_{ij}^{a\kappa,b\kappa'}$ describes minus the force along direction j on atom b in cell κ' generated by a unit displacement along direction i of atom a in cell κ, in the linear regime. The on-site force constants $\Phi_{ij}^{a\kappa,a\kappa}$ are the curvature of the potential well in which the Si or O atoms moves if no other atom is displaced.

The system of coordinates in which the *on-site* force constant tensors will be expressed is one in which these tensors are diagonal: axis 1 is along the [001] direction; axis 2 is along the [110] direction; axis 3 is along the [110] direction. For the other IFC tensors, we adopt the systems of coordinates in which axis 1 is along the bond direction; axis 2 is the orthogonalized direction with respect to axis 1 of the force on atom b due to the displacement of atom a along the axis 1, and axis 3 is perpendicular to axes 1 and 2. (When the force on atom b due to the displacement of atom a is directed along axis 1, axis 2 is defined by orthogonalizing the x axis with respect to axis 1.)

At 0 GPa, the on-site force constants $\Phi_{ii}^{a\kappa,a\kappa}$ for $i=1$, 2, or 3 and $a=$Si are 42.4728, 30.5714, and 25.7465 eV/Å^2, respectively. $\Phi_{ii}^{a\kappa,a\kappa}$ for $i=1$, 2, or 3 and $a=$O are 26.1235, 35.1281, 12.7702 eV/Å^2, respectively. At 73 GPa, the on-site force constants $\Phi_{ii}^{a\kappa,a\kappa}$ for $i=1$, 2, or 3 and $a=$Si are 49.9070, 24.9423, and 24.2650 eV/Å^2, respectively. $\Phi_{ii}^{a\kappa,a\kappa}$ for $i=1$, 2, or 3 and $a=$O are 53.8233, 20.2034, 7.8870 eV/Å^2, respectively. The extremal ratio between $\Phi_{ii}^{a\kappa,a\kappa}$ for $i=1$, 2, or 3 and $a=$Si increases from a factor of 1.65 to a factor of 2.06 when the pressure increases from 0 to 73 GPa. For O atoms, the difference rises from 2.75 to 6.82. $\Phi_{11}^{a\kappa,a\kappa}$ for $a=$O at 73 GPa becomes more than twice as large as the one that is the largest on-site force constant tensor element at 0 GPa. $\Phi_{22}^{a\kappa,a\kappa}$ and $\Phi_{33}^{a\kappa,a\kappa}$ for $a=$O atom shows a decrease by 42 and 38% from 0 to 73 GPa. $\Phi_{33}^{a\kappa,a\kappa}$ for $a=$O atom is the smallest element, indicating that the motion of O atoms out of the plane formed by the three neighboring Si atoms is even easier at 73 GPa than that at 0 GPa, in agreement with the softening of the B_{1g} mode.

The longitudinal IFC $\Phi_{11}^{a\kappa,b\kappa'}$ for $a=$Si and $b=$O nearest neighbor atoms with bond lengths 1.66 and 1.68 Å are -15.9907 and -14.2668 eV/Å^2, respectively, much larger than their counterparts at 0 GPa (-7.9929 and -4.7579 eV/Å^2 with bond lengths 1.75 and 1.77 Å, respectively). The transverse IFC's $\Phi_{33}^{a\kappa,b\kappa'}$ for $a=$Si and $b=$O

TABLE V. The longitudinal ($\Phi_{11}^{a\kappa,b\kappa'}$) and the two transverse ($\Phi_{22}^{a\kappa,b\kappa'}$ and $\Phi_{33}^{a\kappa,b\kappa'}$) interatomic atomic force constants of stishovite for different pairs of atoms at 0 GPa. The longitudinal interatomic force constants $\Phi_{11}^{a\kappa,b\kappa'}$ are decomposed into dipole-dipole and short-range parts (see text), while their values from pair potentials of Refs. 49 and 50 are also mentioned. Interatomic distances d are in Å and force constants are in eV/Å^2.

d	$\Phi_{11}^{a\kappa,b\kappa'}$	$\Phi_{22}^{a\kappa,b\kappa'}$	$\Phi_{33}^{a\kappa,b\kappa'}$	Dipole-dipole	Short range	Ref. 49	Ref. 50
				Si—O			
1.75	−7.9929	−2.6088	−1.3605	13.5253	−21.5182	−6.5054	−5.2436
1.79	−4.7579	−1.2162	−2.0140	15.1346	−19.8915	−3.7046	−2.2017
3.14	0.9397	−0.4465	−0.7488	1.4344	−0.4946	2.9187	3.1714
3.20	1.4392	−0.6010	−0.4135	2.3255	−0.8863	2.7416	2.9614
3.68	0.9834	−0.5233	−0.2740	1.1603	−0.1769	1.7511	1.8283
4.07	2.3566	−0.0913	−0.1166	1.2828	1.0738	1.2715	1.3065
4.11	1.1010	−0.2663	−0.1161	0.7813	0.3197	1.2261	1.2580
4.15	0.9368	−0.3537	−0.1370	1.0087	−0.0709	1.1968	1.2269
4.86	0.5539	−0.2337	−0.0831	0.7152	−0.1613	0.7327	0.7412
4.90	0.5772	−0.1501	−0.0534	0.6151	−0.0379	0.7152	0.7232
5.18	0.4742	−0.1084	−0.1176	0.4742	0.0000	0.6010	0.6060
5.26	0.3673	−0.1448	−0.0909	0.4431	−0.0758	0.5755	0.5800
5.55	0.4179	−0.0709	−0.0962	0.4179	0.0000	0.4889	0.4919
5.61	0.3907	−0.1181	−0.0637	0.4150	−0.0253	0.4734	0.4761
6.11	0.2167	−0.0758	−0.0743	0.2167	0.0000	0.3651	0.3665
6.12	0.1856	−0.0879	−0.0714	0.1856	0.0000	0.3633	0.3646
6.15	0.3061	−0.0549	−0.0719	0.3061	0.0000	0.3577	0.3590
6.17	0.3761	−0.0496	−0.0442	0.3090	0.0671	0.3540	0.3552
6.17	0.2818	−0.0724	−0.0617	0.2692	0.0126	0.3538	0.3550
6.40	0.2585	−0.0593	−0.0622	0.2585	0.0000	0.3170	0.3179
				O—O			
2.28	−9.2669	0.4047	0.4368	−4.3118	−4.9551	−12.7502	−12.9813
2.50	−3.9571	0.3042	0.3979	−2.0786	−1.8785	−8.2750	−8.4713
2.66	−2.2788	0.4120	0.1429	−1.9076	−0.3722	−5.9641	−6.1552
3.00	−0.3693	0.3358	0.2245	−0.6045	0.2352	−2.9616	−3.1136
3.50	−0.4801	0.3173	0.1088	−0.9796	0.4985	−1.2337	−1.3113
3.57	−0.6385	0.0739	0.2221	−1.1214	0.4830	−1.1148	−1.1841
4.01	−0.2429	0.2133	0.0709	−0.3615	0.1186	−0.6681	−0.7013
4.14	−0.2808	0.0836	0.1521	−0.4130	0.1322	−0.5889	−0.6150
4.43	−0.4315	0.1356	0.0923	−0.3430	−0.0875	−0.4644	−0.4799
4.45	−0.5452	0.0466	0.0661	−0.5150	−0.0301	−0.4558	−0.4707
4.51	−0.3207	0.0564	0.0875	−0.3780	0.0573	−0.4357	−0.4490
4.92	−0.3518	0.0729	0.0243	−0.2604	−0.0904	−0.3339	−0.3404
5.21	−0.2128	0.0564	0.0573	−0.2128	0.0000	−0.2813	−0.2853
5.32	−0.3187	0.0598	0.0598	−0.2381	−0.0797	−0.2658	−0.2691
5.78	−0.1633	0.0792	0.0233	−0.1963	0.0330	−0.2081	−0.2097
5.81	−0.1516	0.0476	0.0437	−0.1671	0.0155	−0.2056	−0.2071
5.85	−0.2449	0.0185	0.0457	−0.2546	0.0097	−0.2010	−0.2024
5.97	−0.1866	0.0214	0.0384	−0.1866	0.0000	−0.1895	−0.1907
6.10	−0.1186	0.0583	0.0248	−0.1312	0.0126	−0.1782	−0.1792
6.28	−0.0739	0.0432	0.0330	−0.0739	0.0000	−0.1638	−0.1645
6.37	−0.1244	0.0345	0.0316	−0.1244	0.0000	−0.1576	−0.1583
				Si—Si			
2.66	−8.3525	2.2949	2.2949	−7.6305	−0.7220	−8.4433	
3.21	−5.0027	1.3163	0.5578	−3.7637	−1.2390	−4.9086	
4.14	−1.4518	0.6195	0.3853	−1.7191	0.2672	−2.3277	
4.92	−0.9621	0.3858	0.3270	−1.0729	0.1098	−1.3908	
4.95	−1.1904	0.2196	0.1754	−1.1195	−0.0709	−1.3686	
5.32	−0.8144	0.3051	0.3051	−0.9533	0.1390	−1.1030	
5.85	−0.9582	0.1137	0.1647	−0.7259	−0.2323	−0.8263	

TABLE VI. Same in Table V except at 73 GPa.

d	$\Phi_{11}^{a\kappa,b\kappa'}$	$\Phi_{22}^{a\kappa,b\kappa'}$	$\Phi_{33}^{a\kappa,b\kappa'}$	Dipole-dipole	Short ranged	Ref. 49	Ref. 50
				Si—O			
1.66	−15.9907	−2.3984	−3.5072	17.9090	−33.8988	−16.0565	−15.4460
1.68	−14.2668	−3.2686	−2.7035	15.2424	−29.5092	−13.9419	−13.2182
2.97	1.0874	−0.5768	−0.0729	1.8114	−0.7240	3.5056	3.8827
3.04	1.6355	−0.4154	−0.0850	2.6666	−1.0320	3.2468	3.5662
3.46	1.1904	0.0316	−0.2925	1.3770	−0.1856	2.1273	2.2500
3.85	2.3177	−0.1521	−0.2750	1.4373	0.8804	1.5084	1.5620
3.91	1.2886	−0.2002	−0.2269	0.9494	0.3392	1.4412	1.4891
3.97	1.0427	−0.0792	−0.1463	1.1428	−0.1011	1.3712	1.4135
4.60	0.6802	−0.0748	−0.0967	0.7434	−0.0632	0.8672	0.8803
4.62	0.6443	−0.0199	−0.0578	0.8037	−0.1603	0.8566	0.8694
4.91	0.5520	−0.0700	−0.0568	0.5520	0.0000	0.7111	0.7189
4.99	0.4392	−0.0904	−0.0335	0.5160	−0.0768	0.6737	0.6805
5.21	0.4976	−0.0496	−0.0578	0.4976	0.0000	0.5920	0.5969
5.35	0.4441	−0.0807	−0.0350	0.4733	−0.0282	0.5449	0.5488
5.76	0.2371	−0.0520	−0.0428	0.2371	0.0000	0.4363	0.4385
5.77	0.2614	−0.0428	−0.0462	0.2614	0.0000	0.4352	0.4374
5.80	0.3625	−0.0379	−0.0418	0.3625	0.0000	0.4279	0.4299
5.84	0.4305	−0.0705	−0.0413	0.3625	0.0671	0.4186	0.4206
5.89	0.3285	−0.0369	−0.0603	0.3158	0.0126	0.4077	0.4095
				O—O			
2.19	−10.9928	0.1045	0.6530	−4.6383	−6.3555	−14.8091	−15.1125
2.36	−5.5722	0.3907	0.5238	−2.3867	−3.1855	−10.9446	−11.1509
2.54	−2.7191	0.7492	0.2425	−2.1671	−0.5520	−7.5664	−7.7617
2.82	−0.5325	0.3970	0.2760	−0.7930	0.2614	−4.2837	−4.4608
3.32	−0.7045	0.0627	0.0734	−1.3284	0.6239	−1.6304	−1.7317
3.36	−0.5685	0.0938	0.0398	−1.0923	0.5228	−1.5425	−1.6390
3.79	−0.3187	0.0564	0.1360	−0.4558	0.1360	−0.8390	−0.8869
3.90	−0.3654	0.0972	0.0224	−0.5248	0.1594	−0.7454	−0.7854
4.19	−0.6103	0.1409	−0.0068	−0.5996	−0.0107	−0.5647	−0.5888
4.20	−0.4558	0.0058	0.0428	−0.3984	−0.0573	−0.5565	−0.5799
4.30	−0.3605	0.0457	0.0816	−0.4315	0.0700	−0.5112	−0.5307
4.66	−0.4587	0.0539	0.0870	−0.3207	−0.1380	−0.3948	−0.4051
4.89	−0.2536	0.0277	0.0345	−0.2536	0.0000	−0.3398	−0.3466
5.09	−0.3071	0.0389	0.0389	−0.2711	−0.0360	−0.3019	−0.3067
5.52	−0.2760	0.0117	0.0189	−0.2906	0.0146	−0.2388	−0.2412
5.53	−0.1769	0.0160	0.0185	−0.1905	0.0136	−0.2366	−0.2389
5.54	−0.1895	0.0238	0.0107	−0.2225	0.0321	−0.2356	−0.2379
5.67	−0.2206	0.0199	0.0224	−0.2206	0.0000	−0.2210	−0.2228
5.82	−0.1429	0.0160	0.0287	−0.1565	0.0136	−0.2048	−0.2063
5.93	−0.0972	0.0282	0.0194	−0.0972	0.0000	−0.1932	−0.1944
6.00	−0.1399	0.0131	0.0189	−0.1399	0.0000	−0.1871	−0.1883
6.07	−0.1419	0.0155	0.0175	−0.1419	0.0000	−0.1808	−0.1818
				Si—Si			
2.54	−9.7655	0.4718	0.4718	−8.6693	−1.0962	−9.5110	
3.04	−5.9327	0.2765	0.9494	−4.4751	−1.4577	−5.7860	
3.90	−1.8065	0.0418	0.3528	−2.0660	0.2595	−2.7780	
4.66	−1.1525	0.0913	0.0345	−1.2692	0.1176	−1.6382	
4.71	−1.3799	0.2075	0.2561	−1.2954	−0.0845	−1.5846	
5.09	−0.9387	0.0500	0.0500	−1.0835	0.1448	−1.2563	
5.52	−1.0243	0.0943	0.0986	−0.8260	−0.1982	−0.9875	

atoms with 1.66 Å, and $\Phi_{22}^{a\kappa,b\kappa'}$ for $a=$Si and $b=$O atoms with 1.68 Å also show a large increase. The IFC's between the nearest pair of Si-Si and O-O atoms and the farther pairs of atoms show minor changes between 0 and 73 GPa.

When we decompose the longitudinal components of the IFC's into the long-range dipole-dipole interaction part and short-ranged part, we find an increase by 58% of the short-ranged part of the IFC's between the closest Si-O atoms, because the covalent bond due to the electronic overlap is stronger due to the shorter interatomic distance. In order to estimate the range of the covalent IFC's, we compute the phonon frequencies including short-range forces restricted to pairs of atoms within some cutoff distance. The spatial range of the covalent IFC's is found to be of the order of 5.5 Å at 73 GPa, longer than that at 0 GPa, which is of the order of 4.4 Å. Empirical force constants from Refs. 49 and 50 slightly overestimate *ab initio* IFC's at large distance at both 0 and 73 GPa.

F. The pressure dependence of the elastic properties

So far, we have studied the dielectric properties of stishovite under the assumption that the tetragonal symmetry of the rutile structure is preserved within the investigated pressure region. However, the low-frequency dielectric permittivity tensor is not defined because the B_{1g} mode at the Γ point has an imaginary frequency at 114 GPa. One of the long-wavelength acoustic modes along the Γ-M line in the BZ has an imaginary frequency at 73 GPa. The analysis of the IFC's at 73 GPa show that the mode B_{1g}, with motion of O atoms out of the plane formed by the three neighboring Si atoms, is softer than at 0 GPa while other IFC's become much stiffer. Triggered by these facts, we take a close look at the elastic properties as as a function of pressure and characterize the domain of (meta)stability of stishovite in the rutile structure.

We calculate the elastic constants with respect to a homogeneous pure shear deformation with strain tensor $e_{xx}=-e_{yy}$ at 0, 18, 42, 73, and 114 GPa. As mentioned in Sec. III D, this elastic deformation corresponds to the long-wavelength acoustic modes along the Γ-M line. We find that the shear modului[51] due to the deformation are 107.9, 97.7, 67.1, -38.2 GPa at 0, 18, 42, 73 GPa and interpolation predicts negative shear moduli above 64 GPa. This means that the tetragonal rutile-structured stishovite is unstable above 64 GPa, causing spontaneous shear deformation, i.e., ferroelastic structural phase transition toward the orthorhombic $CaCl_2$ structure. This is a good example of the theoretical account by Miller and Axe[52] that an elastic instability must occur in general crystalline solids if a Raman-active mode is soft. Similar structural transformations are known for $CaCl_2$ and $CaBr_2$, that undergo ferroelastic phase transitions, from the rutile structure above 491 K (Ref. 53) and 780 K,[54] respectively, to the $CaCl_2$ structure at lower temperatures.

G. SiO_2 in the $CaCl_2$ structure: Structural properties

The positive shear modulus of stishovite at 0, 18, and 42 GPa confirm the stability of the rutile structure with respect to the shear deformation. Instability of the rutile-structured stishovite is demonstrated by the negative shear modulus at 73 GPa and 114 GPa. To find the minimum-energy geometry at 73 GPa and 114 GPa, we relax the tetragonal symmetry of the unit cell and calculate the energy with respect to lattice constants a and b. When relaxed at 73 GPa, the tetragonal unit cell with $a=b=3.90$ Å and $u=0.3014$ transforms into a lower-symmetry orthorhombic unit cell with $a=3.83$ Å, $b=3.97$ Å, and O atoms at $(u_1,u_2,0)$, $(1-u_1,1-u_2,0)$, $(\frac{1}{2}-u_1,\frac{1}{2}+u_2,\frac{1}{2})$, and $(\frac{1}{2}+u_1,\frac{1}{2}-u_2,\frac{1}{2})$, with the internal parameters $u_1=0.2803$ and $u_2=0.3198$. At 114 GPa, the relaxation leads the tetragonal unit cell with $a=b=3.82$ Å and $u=0.3005$ to the orthorhombic unit cell with $a=3.72$ Å, $b=3.93$ Å, and the internal parameters $u_1=0.2682$ and $u_2=0.3293$. The Si-O bonds rotate by 3.8° and 5.8° off the diagonal in a-b plane at 73 and 114 GPa, respectively. This corresponds to the B_{1g} displacement if the structure remained tetragonal.

The stability of $CaCl_2$ structure is substantiated by calculating the phonon frequency of the soft mode B_{1g} at pressure higher than 64 GPa. The B_{1g} mode in the relaxed $CaCl_2$ structure at 73 GPa is no longer soft with frequency 219.7 cm^{-1}, as shown in Table 2 of Ref. 47, indicating that the $CaCl_2$ structure is stable upon relaxation.

H. SiO_2 in the $CaCl_2$ structure: Dielectric properties and phonon frequencies at the Γ point

Stishovite in the rutile structure at 73 GPa being found unstable, we want to calculate the dielectric permittivity tensors, the Born effective charges, and the phonon frequencies at the Γ point of stishovite in the $CaCl_2$ structure. These quantities in the rutile structure are symmetric with respect to the permutation of x and y axes: phonon frequencies of modes with motion of atoms perpendicular to the z direction are twofold degenerate. In the $CaCl_2$ structure, the degenerate modes separate due to the loss of symmetry. The other modes also undergo changes. The dielectric permittivity tensors and the Born effective charge tensors of stishovite in the $CaCl_2$ structure at 73 GPa are shown in the rightmost column of Table IV. ϵ_{xx}^{∞} and ϵ_{yy}^{∞} in the $CaCl_2$ structure become nondegenerate into a larger and a smaller value than the degenerate ϵ_{xx}^{∞} and ϵ_{yy}^{∞} in the rutile structure; ϵ_{zz}^{∞} increases by 2.9%. $Z_{\tau,xx}^{*}$, $Z_{\tau,yy}^{*}$, $Z_{\tau,xy}^{*}$, and $Z_{\tau,yx}^{*}$ for $\tau=$Si or O atoms in the $CaCl_2$ structure become nondegenerate with a larger and a smaller value than the degenerate value in the rutile structure. $Z_{\tau,zz}^{*}$ slightly decreases.

The phonon frequencies at the Γ point in the $CaCl_2$ structure are presented in Table 2 of Ref. 47. Each of the doubly degenerate E_u and E_g modes in the rutile structure splits in the $CaCl_2$ structure. The frequencies of the nondegenerate modes in the rutile structure decrease in the $CaCl_2$ structure except the B_{1g} and A_{2g} modes. The frequency of the soft B_{1g} mode in the rutile structure drastically increases to 219.7 cm^{-1} in the $CaCl_2$ structure.

IV. CONCLUSION

The dielectric properties and the lattice dynamics of stishovite are investigated as a function of pressure using the variational DFPT. The low-frequency and high-frequency dielectric permittivity tensors and the Born effective charge tensors are found to be less anisotropic at higher pressure, indicating the local environments of stishovite in the rutile

structure, more compressible along the *a* axis than along *c* axis at high pressure, is less anisotropic. The phonon frequencies of each mode at the Γ point are calculated as a function of pressure and the derived pressure shifts, the Grüneisen parameters, and the LO-TO splittings agree well with experiment. The interpolated frequency of the B_{1g} mode is supposed to vanish at 86 GPa if the rutile structure is maintained. But the phonon band structure at 73 GPa shows an instability of the rutile structure under shear deformation. From the real-space IFC's, we find the motion of the O atom out of the plane formed by the nearest neighbor Si atoms especially easy at 73 GPa, whereas the longitudinal components between a pair of the nearest neighbor Si and O atoms are much larger at 73 GPa than at 0 GPa. The study of the elastic constants with respect to the shear deformation show spontaneous structural deformation at 64 GPa, suggesting a pressure-induced phase transition of the teteragonal rutile-structured stishovite into the orthorhombic $CaCl_2$ structure. We also confirm the instability of stishovite in the rutile structure by structural relaxation.

ACKNOWLEDGMENTS

This work is supported by Korea Science and Engineering Foundation Grant No. 961-0207-043-2, Ministry of Science and Technology R & D Project, and Center for Theoretical Physics in Seoul National University (C.L.), and FNRS-Belgium, the Crédit FRFC 9.4532.93 (Loterie Nationale), and the research contract between UCL, FUNDP, and IBM (X.G.).

[1] R. B. Sosman, *The Phases of Silica* (Rutgers University Press, New Brunswick, 1965).
[2] L. Coes, Science **118**, 131 (1953).
[3] S. M. Stishov and S. V. Popova, Geochemistry **10**, 923 (1961).
[4] S. Akimoto, T. Yagi, and K. Inoue, in *High-Pressure Research: Applications to Geophysics*, edited by M. H. Manghnani and S. Akimoto (Academic, San Diego, 1977), p. 585.
[5] D. M. Teter *et al.*, Phys. Rev. B **52**, 8064 (1995).
[6] D. W. McComb and A. Howie, Nucl. Instrum. Methods Phys. Res. B **96**, 569 (1995).
[7] Q. Williams, R. J. Hemley, M. B. Kruger, and R. Jeanloz, J. Geophys. Res. **98**, 22 157 (1993).
[8] V. Swamy, S. K. Saxena, B. Sundman, and J. Zhang, J. Geophys. Res. **99**, 11 787 (1994).
[9] X. Gonze, Phys. Rev. B **55**, 10 337 (1997).
[10] X. Gonze and C. Lee, Phys. Rev. B **55**, 10 355 (1997).
[11] C. Lee and X. Gonze, Phys. Rev. Lett. **72**, 1686 (1994); Phys. Rev. B **51**, 8610 (1995); C. Lee, *ibid.* **54**, 8973 (1996).
[12] Y. Tsuchida and T. Yagi, Nature (London) **340**, 217 (1989).
[13] R. J. Hemley, in *High-Pressure Research in Mineral Physics*, edited by M. H. Manghnani and Y. Syono (Terra Scientific, Tokyo, 1987), p. 347.
[14] K. J. Kingma, R. E. Cohen, R. J. Hemley, and H.-K. Mao, Nature (London) **347**, 243 (1995).
[15] C. Lee and X. Gonze, J. Phys.: Condens. Matter **7**, 3693 (1995).
[16] L. V. Al'tshuler, M. A. Podurets, G. V. Simakov, and R. F. Trunin, Sov. Phys. Solid State **15**, 969 (1973); M. A. Podurets, G. V. Simakov, and R. F. Trunin, Izv. Acad. Sci. USSR, Phys. Solid Earth **26**, 295 (1990).
[17] K. T. Park, K. Terakura, and Y. Matsui, Nature (London) **336**, 670 (1988).
[18] V. N. German, M. A. Podurets, and R. F. Trunin, Sov. Phys. JETP **37**, 107 (1973).
[19] L. C. Ming and M. H. Manghnani, in *High-Pressure Research in Geophysics*, edited by S. Akimoto and M. H. Manghnani (Academic, Tokyo, 1982), p. 329.
[20] L. Liu, W. A. Bassett, and J. Sharry, J. Geophys. Res. **83**, 2301 (1978).
[21] L. Liu, in *High-Pressure Research in Geophysics* (Ref. 19), p. 349.
[22] M. E. Striefler, EOS Trans. Am. Geophys. Union **66**, 358 (1985).
[23] R. J. Hemley, M. J. Jackson, and R. G. Gordon, EOS Trans. Am. Geophys. Union **66**, 358 (1985).
[24] S. Tsuneyuki, Y. Matsui, H. Aoki, and M. Tsukada, Nature (London) **339**, 209 (1989).
[25] D. M. Sherman, J. Geophys. Res. **98**, 11 865 (1993).
[26] D. J. Lacks and R. G. Gordon, J. Geophys. Res. **98**, 22 147 (1993).
[27] R. E. Cohen, in *High-Pressure Research: Application to Earth and Planetary Sciences*, edited by Y. Syono and M. H. Manghnani (Terra Scientific, Tokyo, 1992), p. 425.
[28] B. B. Karki *et al.*, Phys. Rev. B **55**, 3465 (1997).
[29] P. Hohenberg and W. Kohn, Phys. Rev. **136**, B864 (1964); W. Kohn and L. J. Sham, *ibid.* **140**, A1133 (1965).
[30] W. Pickett, Comput. Phys. Rep. **9**, 115 (1989).
[31] P. Giannozzi, S. de Gironcoli, P. Pavone, and S. Baroni, Phys. Rev. B **43**, 7231 (1991).
[32] X. Gonze, D. C. Allan, and M. P. Teter, Phys. Rev. Lett. **68**, 3603 (1992).
[33] X. Gonze, D. C. Allan, and M. P. Teter, in *Phonon Scattering in Condensed Matter VII*, edited by M. Meissner and R. O. Pohl (Springer-Verlag, Berlin, 1993), pp. 511–512.
[34] X. Gonze, J.-C. Charlier, D. C. Allan, and M. P. Teter, Phys. Rev. B **50**, 13 035 (1994).
[35] C. Lee, Ph. Ghosez, and X. Gonze, Phys. Rev. B **50**, 13 379 (1994).
[36] C. Lee and X. Gonze, Phys. Rev. B **49**, 14 730 (1994).
[37] G.-M. Rignanese, J.-P. Michenaud, and X. Gonze, Phys. Rev. B **53**, 4488 (1996).
[38] Ph. Ghosez, X. Gonze, and J.-P. Michenaud, Ferroelectrics **153**, 91 (1994); Ph. Ghosez, X. Gonze, Ph. Lambin, and J.-P. Michenaud, Phys. Rev. B **51**, 6765 (1995); Ph. Ghosez, X. Gonze, and J.-P. Michenaud, Ferroelectrics **164**, 113 (1995); Ph. Ghosez, X. Gonze, and J.-P. Michenaud, Europhys. Lett. **33**, 713 (1996); Ph. Ghosez, X. Gonze, and J.-P. Michenaud, Ferroelectrics (to be published).
[39] D. M. Ceperley and B. J. Alder, Phys. Rev. Lett. **45**, 566 (1981).
[40] M. C. Payne, M. P. Teter, D. C. Allan, T. A. Arias, and J. D. Joannopoulos, Rev. Mod. Phys. **64**, 1045 (1992).
[41] M. Teter, Phys. Rev. B **48**, 5031 (1993).
[42] H. J. Monkhorst and J. D. Pack, Phys. Rev. B **13**, 5188 (1976).
[43] See, for example, M. Lax, *Symmetry Principles in Solid State and Molecular Physics* (Wiley, New York, 1974), p. 446.
[44] F. D. Murnaghan, Proc. Natl. Acad. Sci. USA **30**, 244 (1944).

[45] N. R. Keskar, N. Troullier, J. L. Martins, and J. R. Chelikowsky, Phys. Rev. B **44**, 4081 (1991).
[46] M. E. Striefler and G. R. Barsch, Phys. Status Solidi B **67**, 143 (1975).
[47] C. Lee and X. Gonze, J. Phys.: Condens. Matter **7**, 3693 (1995).
[48] C. Kittel, *Introduction to Solid State Physics*, 7th ed. (Wiley, New York, 1996), p. 89.
[49] S. Tsuneyuki, M. Tsukada, H. Aoki, and Y. Matsui, Phys. Rev. Lett. **61**, 869 (1988).
[50] B. W. H. van Beest, G. J. Kramer, and R. A. van Santen, Phys. Rev. Lett. **64**, 1955 (1990).
[51] L. D. Landau and E. M. Lifshitz, *Theory of Elasticity* (Pergamon, Oxford, 1986), p. 10.
[52] P. B. Miller and J. D. Axe, Phys. Rev. **163**, 924 (1967).
[53] H.-G. Unruh, D. Mühlenberg, and Ch. Hahn, Z. Phys. B **86**, 133 (1992).
[54] Ch. Hahn and H.-G. Unruh, Phys. Rev. B **43**, 12 665 (1991).
[55] D. R. Hamann, Phys. Rev. Lett. **76**, 660 (1996).
[56] J. S. Tse, D. D. Klug, and D. C. Allan, Phys. Rev. B **51**, 16 392 (1995).
[57] N. L. Ross, J. Shu, R. M. Hazen, and T. Gasparik, Am. Mineral. **75**, 739 (1990).
[58] R. J. Hill, M. D. Newton, and G. V. Gibbs, J. Solid State Chem. **47**, 185 (1983).
[59] W. Sinclair and A. E. Ringwood, Nature (London) **272**, 714 (1978).
[60] B. Olinger, J. Geophys. Res. **81**, 5341 (1976).
[61] L. Liu, W. A. Bassett, and T. Takahashi, J. Geophys. Res. **79**, 1160 (1974).
[62] D. C. Allan and M. P. Teter, J. Am. Ceram. Soc. **73**, 3247 (1990).